# Room-Temperature Nonvolatile Memory Based on a Single-Phase Multiferroic Hexaferrite

*Kun Zhai, Da-Shan Shang, Yi-Sheng Chai, Gang Li, Jian-Wang Cai, Bao-Gen Shen, and Young Sun\**

The cross-coupling between electric polarization and magnetization in multiferroic materials provides a great potential for creating next-generation memory devices. Current studies on magnetoelectric (ME) applications mainly focus on ferromagnetic/ferroelectric heterostructures because single-phase multiferroics with strong magnetoelectric coupling at room temperature are still very rare. Here a type of nonvolatile memory device is presented solely based on a single-phase multiferroic hexaferrite $Sr_3Co_2Fe_{24}O_{41}$ which exhibits nonlinear magnetoelectric effects at room temperature. The principle is to store binary information by employing the states (magnitude and sign) of the first-order and the second-order magnetoelectric coefficients ($\alpha$ and $\beta$), instead of using magnetization, electric polarization, and resistance. The experiments demonstrate repeatable nonvolatile switch of $\alpha$ and $\beta$ by applying pulsed electric fields at room temperature, respectively. Such kind of memory device using single-phase multiferroics paves a pathway toward practical applications of spin-driven multiferroics.

## 1. Introduction

The information era has a strong request for high-performance next-generation memory devices. Several potential candidates include magnetic random-access memory,[1] resistive memory,[2] phase-change memory,[3] and ferroelectric (FE) memory.[4,5] Multiferroic materials combining magnetic and FE orders may show mutual control of electric polarization ($P$) by a magnetic field ($H$) and magnetization ($M$) by an electric field ($E$), which also provide possibilities for creating next-generation information storage devices.[6–9] The magnetoelectric (ME) coupling effects can be described by the ME coefficients $\alpha$, $\beta$, and $\gamma$[10–12]

$$F(E,H) = -PE - \mu_0 MH - \frac{1}{2}\varepsilon_0\varepsilon E^2 - \frac{1}{2}\mu_0\mu H^2$$
$$-\alpha EH - \frac{1}{2}\beta EH^2 - \frac{1}{2}\gamma E^2 H + \dots \tag{1}$$

where $\alpha$ is the first-order (linear) ME coefficient, $\beta$ and $\gamma$ are the second-order coefficients related to derivation of $H$ and $E$, respectively. In most of the studies, only the linear ME coefficient $\alpha$ is concerned.

Recently, we proposed that the states (magnitude and sign) of the ME coefficient $\alpha$ can be used to implement a new type of nonvolatile memory,[8,9] which is in contrast to other memory devices where the states of magnetization, electric polarization, and resistance are usually used to store binary information. The information is written electrically by applying voltage pulses and read out parallelly by inputting a low magnetic field. We have demonstrated experimentally this type of nonvolatile memory based on the nonlinear ME effects in a series of multiferroic heterostructures.[8,9,13,14] Moreover, the second-order coefficients $\beta$ and $\gamma$ which reflect the concavity of the $P$–$H$ or $M$–$E$ curve in local regions may also be used to encode binary information and implement nonvolatile memory when the states of $\beta$ and $\gamma$ can be controlled by external $E$ fields.

In this work, we apply the above principle of memory to single-phase multiferroics. We find that the Z-type hexaferrite $Sr_3Co_2Fe_{24}O_{41}$ (SCFO) single crystal exhibiting nonlinear ME effects at room temperature exactly fulfill the requirement for implementing nonvolatile memory. A simple memory device based on SCFO is demonstrated where the states of the ME coefficient $\alpha$ and $\beta$ can be switched by $E$ field pulses in a nonvolatile way.

Multiferroic hexaferrites are among the most promising candidates of single-phase multiferroics for applications, where spin-driven multiferroicity and strong ME effects are produced due to the complex noncollinear and collinear magnetic

K. Zhai, Dr. D.-S. Shang, Dr. Y.-S. Chai, G. Li, Prof. J.-W. Cai,
Prof. B.-G. Shen, Prof. Y. Sun
Beijing National Laboratory for Condensed Matter Physics
Institute of Physics
Chinese Academy of Sciences
Beijing 100190, P. R. China
E-mail: youngsun@iphy.ac.cn

K. Zhai, G. Li, Prof. J.-W. Cai, Prof. Y. Sun
School of Physical Science
University of Chinese Academy of Sciences
Beijing 100190, P. R. China
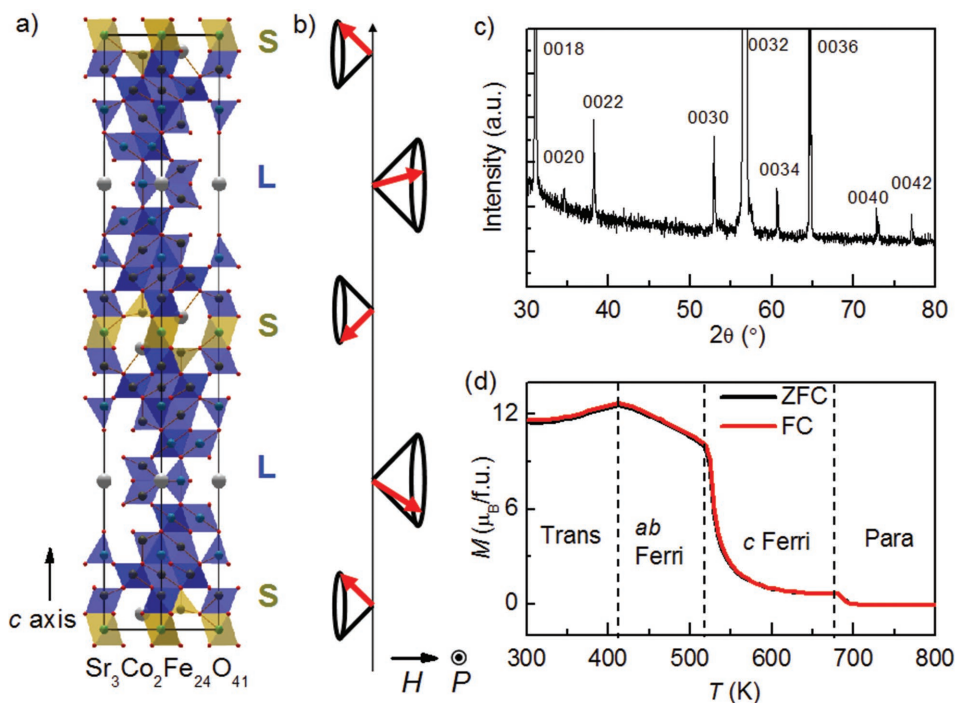
**Figure 1.** a) Crystal structure of Z-type hexaferrites. b) Schematic illustration of transverse conical magnetic structure with in-plane magnetic field $H$ and induced electric polarization $P$. c) Single crystal XRD pattern of $Sr_3Co_2Fe_{24}O_{41}$. d) Temperature dependence of magnetization measured in $H_{ab} = 500$ Oe with zero field cooling and field cooling.

structures.[15–19] The crystal structure of hexaferrites can be classified into several types based on different stacking sequences of S blocks ($Me^{2+}Fe_4O_8$; spinel block), T blocks (($Ba,Sr)_2Fe_8O_{14}$) and R blocks ([($Ba,Sr)Fe_6O_{11}]^{2-}$), such as M-type $BaFe_{12}O_{19}$ (RSR*S*), Y-type $(Ba,Sr)Me_2Fe_{12}O_{22}$ (TSTSTS), Z-type $(Ba,Sr)_3Me_2Fe_{24}O_{41}$ (RSTSR*S*T*S*), and U-type hexaferrites $(Ba,Sr)_4Me_2Fe_{36}O_{60}$ (RSR*S*TS*).[20] Among them, the Z-type hexaferrites with specific chemical compositions are able to show strong ME effects even at room temperature.[21–26]

## 2. Results and Discussion

**Figure 1**a shows the crystal structure of the Z-type hexaferrite SCFO. It can be divided into two different magnetic blocks—large magnetic moment blocks (L) and small magnetic moment blocks (S). In each blocks, the magnetic moment of Fe arrange collinearly.[20] The alternating L and S blocks stack along c-axis, which forms the noncollinear magnetic structure. Previous neutron diffraction on SCFO found that transverse conical spin magnetic structures stabilize below 430 K, which allows finite in-plane $P$ in terms of the inverse Dzyaloshinskii–Moriya mechanism, as shown in Figure 1b.[22]

Figure 1c shows the X-ray diffraction (XRD) patterns of the single crystal of SCFO at room temperature. The c-axis constant is 52.18 Å consistent with previous result.[21] Figure 1d presents the M–T curves in the temperature range of 300–800 K after zero field cooling (ZFC) and field cooling (FC) procedures with ab-plane $H = 500$ Oe. The increase of magnetization below 670 K indicates that the sample enters into magnetic order state, which is consistent with previous study in polycrystalline

and single crystal samples.[21,22] In this magnetic phase, $\mu_L$ and $\mu_S$ are antiparallel to each other along c-axis. Below 520 K, a kink appears in the M–T curves representing the moments
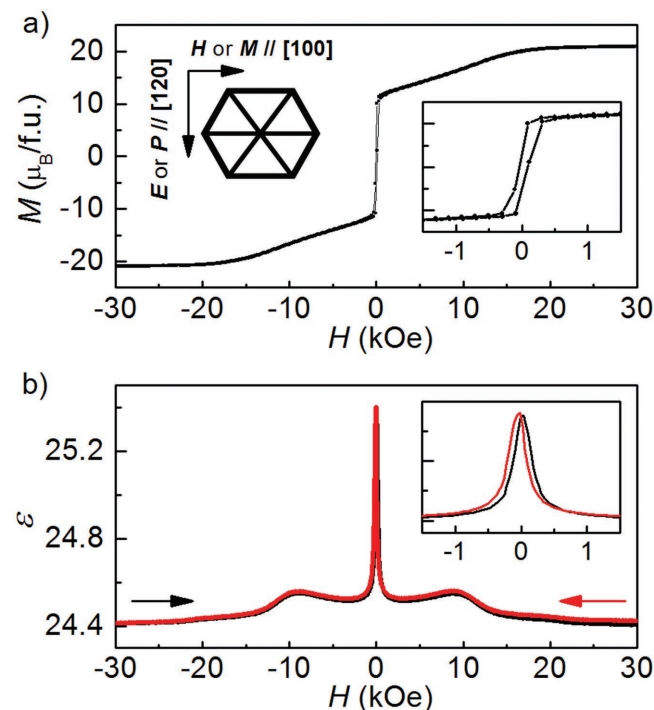


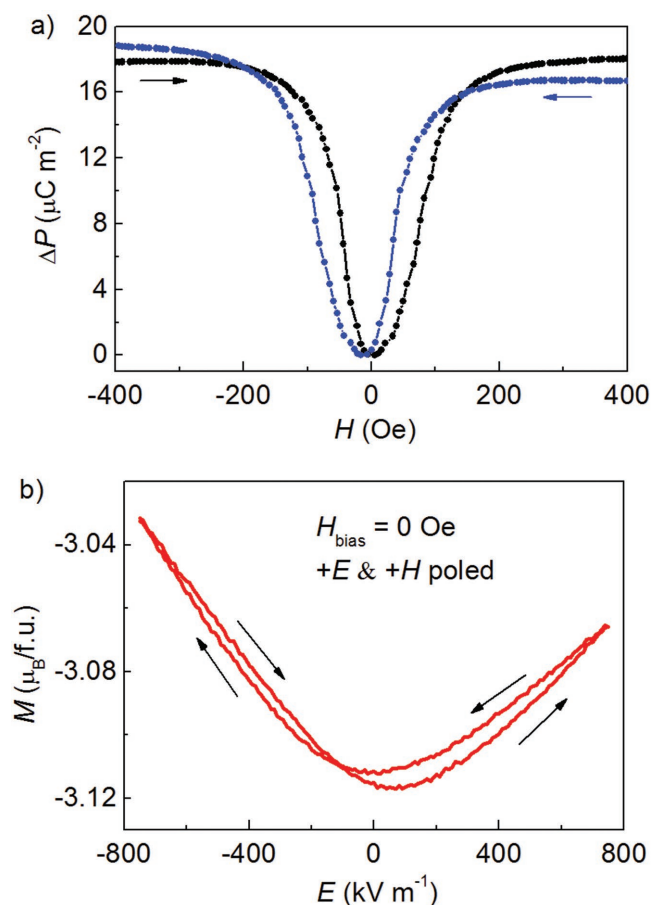**Figure 2.** a) The M–H curve and b) the $\varepsilon$–H curve of $Sr_3Co_2Fe_{24}O_{41}$ at 300 K. The insets show the enlarged view in the low field region. The schematic configuration of measurement is illustrated in (a).

ADVANCED
SCIENCE NEWS
www.advancedsciencenews.com

ADVANCED
FUNCTIONAL
MATERIALS
www.afm-journal.de

rotate from $c$-axis to $ab$ plane. A cusp anomaly was observed around 430 K, which is attributed to the magnetic phase transition into a conical magnetic ordered state and the transition temperature is well above room temperature.[22] The results imply that the application of in-plane $H$ gives rise to polarization via a transverse cone magnetic ordered state, as reported in previous Z-type hexaferrites (Figure 1b).

**Figure 2**a shows the $M–H$ hysteresis loop measured at 300 K and the inset presents the schematic measurement configuration. The saturation magnetization at 30 kOe is 20 $\mu_B$/f.u. consistent with previous study. Figure 2b shows the relative dielectric constant $\varepsilon$ as a function of $H$ at 300 K. The dotted lines marked in Figure 2a distinguished by the derivation of $M$ by $H$ are consistent well with the changes on magnetodielectric curves shown in Figure 2b, which is attributed to a magnetic structure transition from noncollinear at low fields to a ferrimagnetic phase at high fields, accompanying by FE to paraelectric (PE) phase. The sharp dielectric peak around zero field indicates the boundary of two FE states.

**Figure 3**a shows the $\Delta P–H$ curves at room temperature after $+E$ and $+H$ poling conditions. $P$ as a function of $H$ was obtained by integrating the current with respect to time. The maximum polarization is 18 µC m$^{-2}$ and the polarization

is irreversible with a small hysteresis when sweeping $H$ through zero field. Therefore, the $\Delta P–H$ curves show a butterfly shape. We further measured the $E$ field manipulation of magnetization, as shown in Figure 3b. In zero DC bias magnetic field, the variation of magnetization with $E$ field exhibits a parabolic shape, which is mainly attributed to the second ME term. The $M–E$ curve with a hysteresis also shows a butterfly shape. The magnetization is not reversed by $E$ fields, which is different from Y-type hexaferrites.[27,28] The slopes of d$P$/d$H$ and d$M$/d$H$ are the direct ME coefficient ($\alpha_D$) and converse ME coefficient ($\alpha_C$), respectively. The butterfly shape gives opposite sign of the ME coefficient at two branches[29] and thus can be used for nonvolatile memory.

In the following, we demonstrate the nonvolatile switching of $\alpha$ by applying pulse voltages. $\alpha$ was measured by a dynamic method as described in the Supporting Information and schematically shown in Figure S1 in the Supporting Information. The measurement was carried out at 300 K after $+E$ and $+H$ poling procedures. **Figure 4**a shows the ME coefficient $\alpha$ as a function of in-plane DC bias magnetic field. The maximum ME coefficient appears around 100 Oe with a value of 15 mV cm$^{-1}$ Oe$^{-1}$. Figure 4b demonstrates the repeatable switching of $\alpha$ of the device in zero

**Figure 3.** a) Electric polarization as a function of magnetic field at 300 K after $+E$ and $+H$ poling procedure. b) Magnetization as a function of electric field at 300 K after $+E$ and $+H$ poling procedure. No dc bias magnetic field is applied.
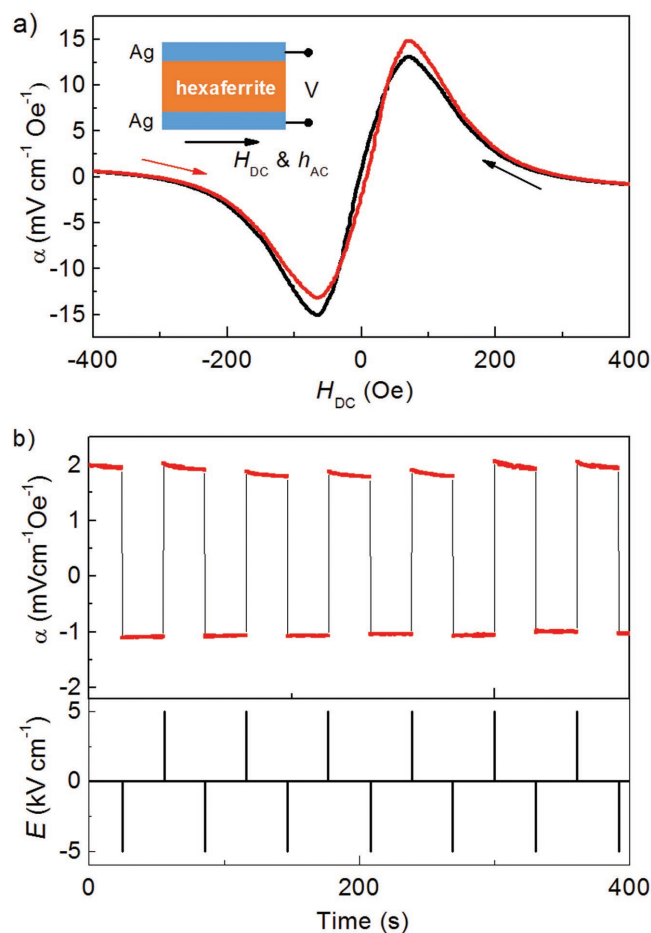
**Figure 4.** a) The first-order ME coefficient $\alpha$ as a function of applied dc magnetic field. The inset shows the structure of device and the configuration of measurements. b) Repeatable switch of the ME coefficient $\alpha$ by applying pulses of electric field in zero dc bias magnetic field.

**ADVANCED
SCIENCE NEWS**
www.advancedsciencenews.com

**ADVANCED
FUNCTIONAL
MATERIALS**
www.afm-journal.de

DC magnetic field. After applying a +500 kV m$^{-1}$ $E$ field, $\alpha_D$ is measured for 40 s; then, a −500 kV m$^{-1}$ $E$ field is applied and $\alpha$ is measured for another 40 s. This process is repeated for several cycles. Two states of $\alpha$ can be clearly distinguished. After applying a positive $E$ pulse $\alpha$ reaches a high state $\alpha$ = 2 mV cm$^{-1}$ Oe$^{-1}$ and retains the state afterward. Only after a negative $E$ pulse is applied $\alpha$ reaches a low state of −1 mV cm$^{-1}$ Oe$^{-1}$. $\alpha$ is the derivation of $P$ by $H$, where $\alpha_H \approx \alpha_E$, which is the slop of $P$–$H$ or $M$–$E$ at specific magnetic field and it is very sensitive to biasing $H$.[22]

By processing the ME voltage with Fourier transform in a lock-in amplifier, we can obtain the higher order coefficient. The second harmonic term of the ME voltage contains $\beta$ as described in Supporting Information. **Figure 5**a shows the magnetic field dependence of $\beta$. A dip-peak-dip feature can be seen and the magnitude of $\beta$ is almost two orders smaller compared with the first order coefficient $\alpha$.

To check the change of remanent polarization at $H$ = 0 under $E$, we denote **1** and **2** as two states at zero electric field after experiencing the +$E$ and −$E$ history, respectively. By sweeping $H$ to positive or negative branch, we obtain the ME current. And $P$ was obtained by integrating the ME current. Figure 5b shows the $P$–$H$ curves under $E$ = 500 kV m$^{-1}$, $E$ = 0, and $E$ = −500 kV m$^{-1}$, respectively. When +$E$ applied the value of electric polarization changes and the concavity around zero field also changes. While when −$E$ applied, the concavity remains. We can see that the electric field can change the concavity around zero field so that the second-order ME coefficient $\beta$ can have two different signs.

Figure 5c demonstrates the repeatable switching of $\beta$ at zero DC bias magnetic field. A similar procedure was applied to measure $\beta$. After applying a +500 kV m$^{-1}$ $E$ field, $\beta$ is measured for 40 s; then, a −500 kV m$^{-1}$ $E$ field is applied and $\beta$ is measured for another 40 s. This process is repeated for several cycles. Two states of $\beta$ can be distinguished. Applying a negative $E$ pulse drives $\beta$ to a positive state of 0.012 mV cm$^{-1}$ Oe$^{-2}$ and a positive $E$ pulse drives it to a low state of −0.12 mV cm$^{-1}$ Oe$^{-2}$. The states of $\beta$ retain after cutting off the $E$ field, showing nonvolatile behavior. $\beta$ is the second derivation of $P$ over $H$, which is the concavity of $P$–$H$ at specific magnetic fields. Compared with the first-order coefficient $\alpha$, the slope of curve, $\beta$ is insensitive to bias DC $H$. This feature could be beneficial for memory devices working under environments with stray magnetic fields. The reversal of concavity of $P$–$H$ under +$E$ as seen in Figure 5b plays a key to obtain the opposite sign of $\beta$. This distortion in $P$–$H$ may be attributed to the $E$ field influence on FE domain structure.

Finally, we discuss on the operation speed of this type of memory. The speed of writing is comparable to that (≈20 ns) of commercial ferroelectric random access memory because the role of applied voltage pulse is to reverse ferroelectric polarization. The reading speed relies on the time measuring the ME coefficients. In the conventional dynamic method, the reading time is inversely proportional to the frequency of applied ac magnetic field. In practical devices, a pulse magnetic field instead of ac magnetic field can be used to induce the ME voltage with a high reading speed.

## 3. Conclusion

In summary, we have demonstrated a type of nonvolatile memory at room temperature based on the nonlinear
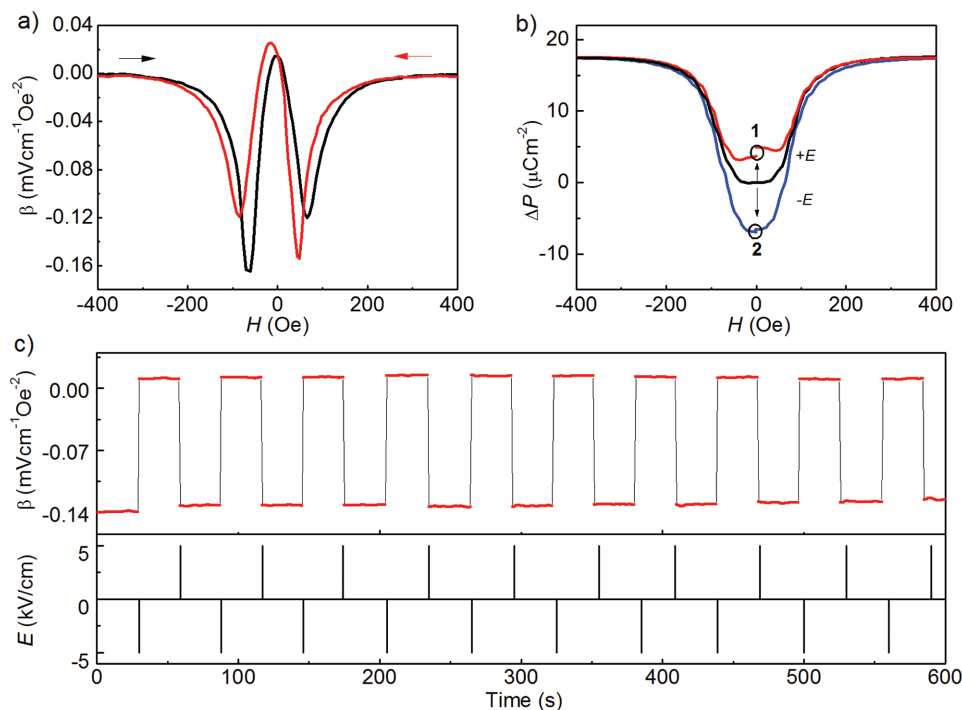


**Figure 5.** a) The second-order ME coefficient $\beta$ as a function of external magnetic field. b) The $P$–$H_{ab}$ curves measured from state 1 and state 2 in (a) after +$E$ and +$H$ poled. c) Repeatable switch of the second-order ME coefficient $\beta$ by pulsed electric field in zero dc bias magnetic field.

ME effects in a single-phase multiferroic hexaferrite (SCFO). Both the first-order and second-order ME coefficients, $\alpha$ and $\beta$, can be employed to store binary information. Repeatable non-volatile switching of $\alpha$ and $\beta$ between high and low states is realized by applying positive and negative $E$ pluses. This kind of memory has the benefits of low energy consumption and simple structure. We expect that quite a number of spin-driven multiferroics could have similar nonlinear ME effects and thus can be used for nonvolatile memory. Our study opens a new door for the practical applications of single-phase multiferroics.

## 4. Experimental Section

*Sample Preparation*: $Sr_3Co_2Fe_{24}O_{41}$ single crystal was synthesized by $Na_2O$-$Fe_2O_3$ flux method with composition of $SrCO_3$, $Co_3O_4$, $Fe_2O_3$, and $Na_2CO_3$. The powders were weighted to the desired chemical compositions and mixed by a mortar. The mixed powders were heated to 1420 °C and kept at that temperature for 20 h to melt the mixture completely following by a thermal cycles to remove spinel nuclei and extra hexaferrites nuclei. Then cooled the mixtures at the rate of 1 °C h$^{-1}$ to 1100 °C to grow Z-type hexaferrite.[22] To elevate the insulating properties of the sample, the sample were annealed at 950 °C for 12 h under 10 atm of pure oxygen.[30] The electrical resistivity of SCFO was greatly improved as shown in Figure S2 in the Supporting Information. The sample was cut into rectangle plate with the dimension of $3 \times 1 \times 0.2$ mm$^3$. The silver paste was painted on the largest faces.

*ME Poling Procedures*: An external magnetic field was set to 30 kOe then ramp to 2 kOe to cross the PE to FE phase boundary, with $E = 500$ kV m$^{-1}$ applied to the samples to align the ferroelectric domains. Then, the $E$ field was turned off and the electrodes were shorted for 30 min before sweeping $H$ to obtain the ME current or ME coefficients.

*Electrical and Magnetic Property Measurements*: The ME current was measured by a high resistance electrometer (Keithley 6517B) and the dielectric constant ($\varepsilon$) was measured by an LCR meter (Agilent 4980A). The polarization was obtained by integrating the ME current with time. The magnetization vs temperature up to 800 K was measured in a Vibrating Sample Magnetometer (DMS Model 4, ADE, Inc.). The magnetization with applied electric fields was measured in a magnetic property measuring system (Quantum Design) using a homemade sample holder.

*The ME Coefficients Measurements*: The ME coefficients $\alpha$ and $\beta$ were measured by a dynamic method as described in details in the Supporting Information.

## Supporting Information

Supporting Information is available from the Wiley Online Library or from the author.

## Conflict of Interest

The authors declare no conflict of interest.

[1] J. Åkerman, *Science* **2005**, *308*, 508.
[2] R. Waser, M. Aono, *Nat. Mater.* **2007**, *6*, 833.
[3] M. Wuttig, N. Yamada, *Nat. Mater.* **2007**, *6*, 824.
[4] V. Garcia, S. Fusil, K. Bouzehouane, S. Enouz-Vedrenne, N. D. Mathur, A. Barthélémy, M. Bibes, *Nature* **2009**, *460*, 81.
[5] R. Guo, L. You, Y. Zhou, Z. S. Lim, X. Zou, L. Chen, R. Ramesh, J. Wang, *Nat. Commun.* **2013**, *4*, 1990.
[6] J. F. Scoot, *Nat. Mater.* **2007**, *6*, 256.
[7] M. Bibes, A. Barthélémy, *Nat. Mater.* **2008**, *7*, 425.
[8] J. Shen, J. Cong, Y. Chai, D. Shang, S. Shen, K. Zhai, Y. Tian, Y. Sun, *Phys. Rev. Appl.* **2016**, *6*, 021001.
[9] J. Shen, J. Cong, D. Shang, Y. Chai, S. Shen, K. Zhai, Y. Sun, *Sci. Rep.* **2016**, *6*, 34473.
[10] M. Fiebig, *J. Phys. D: Appl. Phys.* **2005**, *38* 123.
[11] W. Eerenstein, N. D. Mathur, J. F. Scott, *Nature* **2006**, *442*, 759.
[12] M. Lujan, J.-P. Rivera, S. Kizhaev, H. Schmid, G. Triscone, J. Muller, Z.-G. Ye, B. Mettout, R. Bouzerar, *Ferroelectrics* **1994**, *161*, 77.
[13] J. Shen, D. Shang, Y. Chai, Y. Wang, J. Cong, S. Shen, L. Yan, W. Wang, Y. Sun, *Phys. Rev. Appl.* **2016**, *6*, 064028.
[14] P. Lu, D. Shang, J. Shen, Y. Chai, C. Yang, K. Zhai, J. Cong, S. Shen, Y. Sun, *Appl. Phys. Lett.* **2016**, *109*, 252902.
[15] Y. Tokura, S. Seki, *Adv. Mater.* **2010**, *22*, 1554.
[16] I. A. Sergienko, E. Dagotto, *Phys. Rev. B* **2006**, *73*, 0944343.
[17] H. Katsura, N. Nagaosa, A. V. Balatsky, *Phys. Rev. Lett.* **2005**, *95*, 057205.
[18] Y. J. Choi, H. T. Yi, S. Lee, Q. Huang, V. Kiryukhin, S.-W. Cheong, *Phys. Rev. Lett.* **2008**, *100*, 047601.
[19] S.-P. Shen, X.-Z. Liu, Y.-S. Chai, A. Studer, K. Rule, K. Zhai, L.-Q. Yan, D.-S. Shang, F. Klose, Y.-T. Liu, D.-F. Chen, Y. Sun, *Phys. Rev. B* **2017**, *95*, 094405 .
[20] T. Kimura, *Annu. Rev. Condens. Matter Phys.* **2012**, *3*, 93.
[21] Y. Kitagawa, Y. Hiraoka, T. Hinda, T. Ishikura, H. Nakamura, T. Kimura, *Nat. Mater.* **2010**, *9* 797.
[22] S. H. Chun, Y. S. Chai, B.-G. Jeon, H. J. Kim, Y. S. Oh, I. Kim, H. Kim, B. J. Jeon, S. Y. Haam, J.-Y. Park, S. H. Lee, J.-H. Chung, J.-H. Park, K. H. Kim, *Phys. Rev. Lett.* **2012**, *108*, 177201.
[23] M. Soda, T. Ishikura, H. Nakamura, Y. Wakabayashi, T. Kimura, *Phys. Rev. Lett.* **2011**, *106*, 087201.
[24] K. Okumura, K. Haruki, T. Ishikura, S. Hirose, T. Kimura, *Appl. Phys. Lett.* **2013**, *103*, 032906.
[25] J. Wu, Z. Shi, J. Xu, N. Li, Z. Zheng, H. Geng, Z. Xie, L. Zheng, *Appl. Phys. Lett.* **2012**, *101*, 122903.
[26] F. Kadlec, C. Kadlec, J. Vít, F. Borodavka, M. Kempa, J. Prokleška, J. Buršík, R. Uhrecký, S. Rols, Y. Chai, K. Zhai, Y. Sun, J. Drahokoupil, V. Goian, S. Kamba, *Phys. Rev. B* **2016**, *94*, 024419.
[27] Y. S. Chai, S. Kwon, S. H. Chun, I. Kim, B.-G. Jeon, K. H. Kim, S. Lee, *Nat. Commun.* **2014**, *5*, 4208.
[28] K. Zhai, Y. Wu, S. Shen, W. Tian, H. Cao, Y. Chai, B. C. Chakoumakos, D. Shang, L. Yan, F. Wang, Y. Sun. *Nat. Commun.* **2017**, *8*, 519.
[29] D.-S. Shang, Y.-S. Chai, Z.-X. Cao, J. Lu, Y. Sun, *Chin. Phys. B* **2015**, *24*, 068402.
[30] S. Hirose, K. Haruki, A. Ando, T. Kimura, *J. Am. Ceram. Soc.* **2015**, *98*, 2104.